Flexible Flat Panel Displays, Edited by Gregory P. Crawford.
ISBN 0-471-XXXXX-X

Chapter 12: MECHANICS OF TFT TECHNOLOGY ON FLEXIBLE SUBSTRATES

Sigurd Wagner, Helena Gleskova, I-Chun Cheng, and James C. Sturm

Department of Electrical Engineering and Princeton Institute for the Science and Technology of Materials, Princeton University, Princeton, NJ 08544

Z. Suo
Division of Engineering and Applied Sciences, Harvard University, Cambridge, MA 02139

12.1 Introduction

The effect of mechanical stress on amorphous silicon (a-Si) thin film transistors (TFTs) and material began to be studied in the mid-80s (Jones, 1985, Spear and Heintze, 1986). Research with TFTs on flexible substrates dates back to 1967 (Brody, 1996), and was revived when the commercially important a-Si TFTs were made in the mid-90s on flexible substrates of glass (Gleskova et al., 1995), steel (Theiss and Wagner, 1996) and organic polymers (Constant et al., 1994, Burns et al., 1997, Gleskova et al., 1998, H. Gleskova, 1998, Parsons et al., 1998, Sandoe, 1998, Lueder et al., 1998, Bonse et al., 1998, Theiss et al., 1998). Flexible TFT backplanes are in industrial development (Young et al., 2003). Eventually they may be made by roll-to-roll processing (Wagner et al., 2000). Research on flexible TFT backplanes has been accompanied by studies of the effects of mechanical deformation on the TFTs. By now the basic experimental and theoretical information required for the manufacture and use of flexible TFT backplanes has been developed. We review it with some emphasis on TFTs made of rigid a-Si on compliant substrates of organic polymers.

12.2 Deformation of a thin film transistor backplane

A TFT backplane may be deformed by internally produced forces. These include stresses built-in by film growth, by differential thermal expansion or contraction, and by the uptake or release of humidity. A backplane also may be deformed by an external force that bends it, shapes it conformally, or elastically stretches and relaxes it. We survey how mechanical stress may be applied to or develop in a TFT backplane.

12.2.1 Mechanical stress introduced by shaping a TFT backplane

Thin-film transistor (TFT) backplanes are manufactured flat, to benefit from the tools that have been developed for planar semiconductor fabrication. Then the backplanes are strained to produce various shapes. Figure 12.1 illustrates the three types of electronic surfaces that are subsumed under the concept of "flexible." Bending, flexing, or folding produces the cylinder illustrated in Figure 12.1(a). The strain experienced by the active devices may be small,


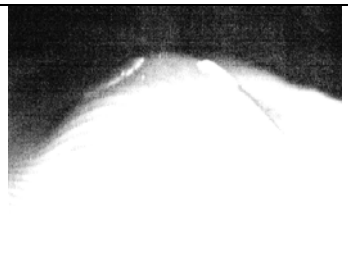


(a) (b) (c)

Figure 12.1 Types of deformation of electronic surfaces: (a) Elastic bending, once or repeatedly, as for a wristband display (Chen, 2001) (b) Conformal shaping by large, one-time, plastic deformation (Pai-hui I. Hsu, 2000). (c) Elastic electronic surfaces for large, repeated, deformation (Lumelsky et al., 2001). In (b) and (c) the devices are placed on rigid islands that are integrated with a deformable substrate.

particularly when the device is placed in the neutral plane. Figure 12.1(b) shows a spherical dome that is produced by out-of-plane deformation. This deformation may be large, may deform the surface permanently by plastic flow, and may not be uniform over the surface. Such shaped surfaces are called deformed, conformal, conformally shaped, or compliant. A third type of electronic surface is shaped in the same way but with the added property that it is elastic, as would be the sensor glove whose concept is shown in Figure 12.1(c). Present industrial development is focused on the bending of flexible TFT backplanes. A spherically shaped TFT circuit of the type shown in Figure 12.1(b) has been demonstrated (Hsu et al., 2002a), and an OLED display has been made on a dome (Bhattacharya et al., 2004). Active electronic surfaces that can undergo large elastic deformation are only beginning to enter research (Lacour et al., 2003, Gray et al., 2004, Wagner et al., 2004). In this chapter we discuss bent and conformally shaped surfaces.

12.2.2 Mechanical stresses introduced during the fabrication of a TFT backplane

TFTs are built on substrates layer-by-layer. Typical layer sequences including substrate planarization and passivation are shown in Figure 12.2 for a backchannel cut amorphous silicon (a-Si) TFT structure. Standard thickness ranges of flexible substrate thicknesses are: glass, 50 μm to 80 μm; organic polymers, 50 μm to 200 μm; and steel, 25 μm to 150 μm. Planarization and passivation layers are 0.2 μm to 1 μm thick, and the TFT is slightly less than 1μm thick.

Even when a TFT backplane is designed to be flat, it experiences stress at many stages during manufacture and use. Built-in stress originates in films that are grown with out-of-

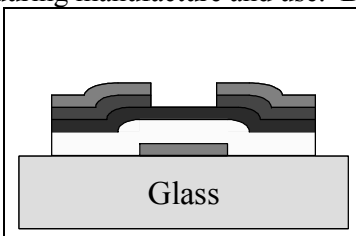

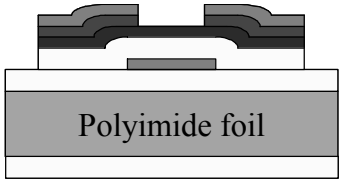

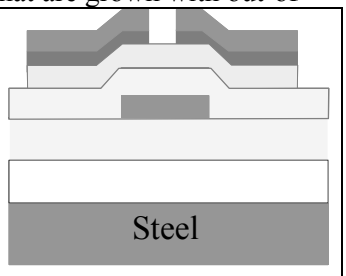

(a) (b) (c)

Figure 12.2 Schematic cross sections of back-channel cut a-Si TFTs on: (a) Glass (Gleskova et al., 1996) (b) Polyimide passivated on both sides with silicon nitride (Gleskova et al., 1998) (c) Steel planarized with spin-on glass and then passivated with silicon nitride (Ma et al., 1997)

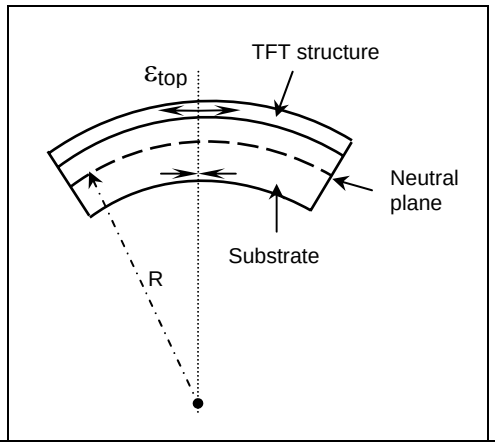

Figure 12.3 A film-on-foil structure bent to a cylindrical roll. When a TFT backplane of thickness *d* is rolled to a radius *r*, the thin film is put into a well defined strain, which is tensile when the film is on the outside of the roll and compressive on the inside

equilibrium atoms that seek to move to low-energy, equilibrium, positions. Thermal and humidity stresses are caused by differences in thermal expansion and humidity coefficients between film and substrate, or between films.

The mechanics of TFT backplanes is understood most easily when device and passivation layers are approximated by a single homogeneous film that completely covers the substrate. This approximation, which simplifies analysis and modeling, does not do justice to layered and patterned devices, but is useful in the frequent absence of detailed information.

The stress σ, a force applied to an area, is the response to the strain ε:

$$\sigma = Y \cdot \varepsilon . \tag{12.1}$$

Y is the elastic modulus. σ and Y have the dimension of pressure and are stated in GPa. ε is dimensionless and frequently is stated in percent. The behavior of the film-on-substrate structure under stress depend strongly on the elastic moduli and thicknesses of the substrate Y_s, d_s and the film Y_f, d_f. Three different situations encountered are listed in Table 12.1. When $Y_f \cdot d_f << Y_s \cdot d_s$, the substrate dominates and the film complies with it, as a TFT does on a plate glass substrate or an OLED on steel. The stress in the substrate is small, and the film/substrate couple curves little or only slightly, even when the film is highly stressed. When $Y_f \cdot d_f >> Y_s \cdot d_s$, the film dominates. This situation has not been encountered in displays but is being reached in electronic skins. A stiff film and a compliant substrate, like a-Si TFT film on an organic polymer foil, may have similar products of elastic modulus and thickness, $Y_f \cdot d_f \approx Y_s \cdot d_s$. Such equal strength of film and substrate gives rise to complicated mechanical situations. The material with the high elastic modulus is called stiff and that with low modulus, compliant. In TFT backplanes, silicon

Table 12.1 Device film / substrate combinations grouped by elastic moduli

		Thin film (small d_f)	
		Stiff (large Y_f)	Compliant (small Y_f)
Thick substrate (large d_s)	Stiff (large Y_s)	Si TFT / glass	OLED / steel
	Compliant (small Y_s)	ITO / polymer	OTFT / polymer

device semiconductors, insulators and metals, and glass and steel substrates with *Y* ranging from ~ 50 GPa to ~ 200 GPa are stiff. Organic polymer substrates and organic semiconductors with *Y* < 5 GPa are compliant.

Structures of silicon TFT films on organic polymer substrates change their curvature throughout circuit fabrication. With this change in curvature comes a change in the size of the work piece. A size change between mask levels, for example the gate level and the source/drain contact level in non-self aligned TFTs, causes misalignment between gate and source/drain. To prevent this misalignment the organic polymer ("plastic") substrate may be bonded to a rigid carrier, of glass or an oxidized silicon wafer. The adhesive used for bonding must withstand the TFT process temperatures and chemicals. If a thermoplastic adhesive is used, its glass temperature must be lower than the glass temperature of the plastic substrate. This use of an adhesive reduces the maximum process temperature from the value that the substrate itself would withstand. Peeling of the finished backplane from the carrier still requires force, which can break the TFTs. In our laboratory we have been working with free-standing substrates that are bonded temporarily only for photolithography.

For a quantitative understanding of the mechanics of a homogeneous stiff film on a compliant substrate, we summarize here the theoretical description of stress, strain and curvature induced by processing or by external force (Gleskova et al., 1998, H. Gleskova, 1998, Suo et al., 1999).

12.3 Stress, strain and curvature of a film / substrate couple

The built-in stress σ_0 in a film arises from a mismatch strain ε_0, which is taken to be positive when it induces a tensile stress in the film. ε_0 is determined experimentally as a function of materials system and deposition condition. The thermal expansion mismatch strain ε_{th} is produced by a temperature change of ΔT and the difference in the thermal expansion coefficients of the film and the substrate, α_f and α_s. The total mismatch strain is the sum of the two contributions:

$$\varepsilon_M = \varepsilon_0 + \left(\alpha_f - \alpha_s\right)\Delta T . \tag{12.2}$$

We assume that this strain is not relaxed by any inelastic process such as plastic deformation of the film or substrate. We now compare the mechanical behavior of a film on a stiff substrate to one on a compliant substrate. (Suo et al., 1999)

12.3.1 Stiff substrate

Because the substrate is stiff, the film must conform to it. A biaxial stress, σ_f, arises in the plane of the film, which relates to the mismatch strain as

$$\sigma_f = \varepsilon_M Y_f^* . \tag{12.3}$$

Here $Y_f^* = Y_f / \left(1 - \nu_f\right)$ is the biaxial elastic modulus of the film, with Y_f being Young's modulus and ν_f Poisson's ratio. The stress in the substrate is much smaller than the stress in the film. The mismatch causes the substrate to bend (Fig. 12.3). The radius of curvature *R* is given

by the well-known Stoney formula (Timoshenko and Goodier, 1970):

$$R = \frac{Y_s^* d_s^2}{6\sigma_f d_f}, \tag{12.4}$$

where d_f is the film thickness, d_s the substrate thickness, and Y_s^* the biaxial elastic modulus of the substrate. Because the substrate is stiff, the radius of curvature is very large. Determining the stress in the film by measuring this radius of curvature is an established practice.

12.3.2 Compliant substrate

When a film is deposited on a thin, compliant substrate, the substrate also deforms considerably. Consequently, *the stress in the film is reduced*. In addition, the radius of curvature *R* can become very small. When during deposition we hold the substrate in a rigid frame, so that the substrate is flat, the stress in the film is given by

$$\sigma_f = \frac{\varepsilon_M Y_f^*}{1 + \left(Y_f^* d_f\right) / \left(Y_s^* d_s\right)}. \tag{12.5}$$

Stiff device films have much higher elastic moduli than the plastic substrate. Therefore, the products $Y_f^* d_f$ and $Y_s^* d_s$ are comparable in magnitude. Consequently, the stress in the film deposited on the thin, compliant substrate is reduced by a factor of about 2 from a film on a stiff substrate. The stress in the film is no longer set by a rigid substrate, but now depends on the substrate thickness and elastic modulus. The stress in the substrate is given by

$$\sigma_s = -\sigma_f d_f \,/\, d_s. \tag{12.6}$$

This stress is still quite small compared to the stress in the film for a thickness ratio $d_f / d_s = 1/50$ (e. g., a 1-µm thick film on a 50-µm thick substrate).

One technique for flattening the substrate is to deposit films of the same thickness on both sides of the substrate, as shown in Figure 12.2(b). The above equations are still applicable, with d_f being the sum of the thicknesses of the two films.

When a film is deposited on a compliant substrate which is held in a frame, and the structure then is released from the frame, the substrate may bend substantially. Although the stresses in the film and the substrate are biaxial, the substrate bends into a roll with a radius of curvature of

$$R = \frac{\left(\bar{Y}_s d_s^2 - \bar{Y}_f d_f^2\right)^2 + 4\bar{Y}_f \bar{Y}_s d_f d_s \left(d_f + d_s\right)^2}{6\varepsilon_M (1+\nu)\bar{Y}_f \bar{Y}_s d_f d_s \left(d_f + d_s\right)}. \tag{12.7}$$

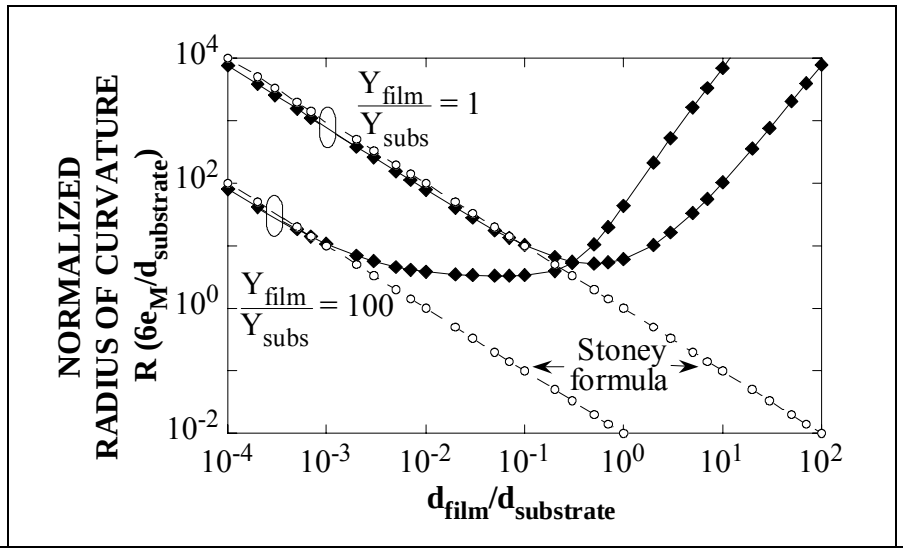

Figure 12.4 Normalized radius of curvature as a function of film/substrate thickness ratio. Two different substrate types are illustrated: glass or steel ($Y_f/Y_s \cong 1$) and organic polymer ($Y_f/Y_s \cong 100$). We assume $\nu_f = \nu_s$. Full lines represent the exact solution of Equation (12.7), dashed lines the approximation for thick, stiff substrate of Equation (12.4) (Gleskova et al., 1998)

Here $\bar{Y} = Y / \left(1 - \nu^2\right)$ is the plane strain elastic modulus (Timoshenko and Goodier, 1970). For a compliant substrate, Eq. (12.7) must be used instead of the Stoney formula (Eq. 12.4), for example, when calculating the mismatch strain from the experimentally determined radius of curvature. Figure 12.4 shows the normalized radius of curvature, calculated using Eq. (12.4) and Eq. (12.7), plotted as a function of the film-to-substrate thickness ratio. In the case of inorganic semiconductors and metals on a glass substrate, $Y_f / Y_s \cong 1$, and the Stoney formula is a good approximation if $d_f / d_s \leq 0.1$. In the case of an organic polymer substrate, $Y_f / Y_s \cong 100$, and the Stoney formula is useful only for $d_f / d_s \leq 0.001$. With typical thicknesses of plastic substrates of 50 μm to 200 μm, $d_f / d_s \cong 0.01$, and Eq. (12.7) must be used. Another important conclusion from Figure 12.4 is that even with a compliant substrate, theoretically there are two regimes when the film/substrate couple is flat, i.e., $R \to \infty$: (1) the film is much thinner than the substrate and therefore must comply with it, and (2) the film is much thicker than the substrate and therefore the substrate must comply with the film.

12.3.3 Bending by externally applied moment

Let us analyze the strain in a blanket film deposited on a stiff foil substrate like steel or glass. Both fabrication process and externally applied bending moment cause strain in the film. We first consider the external bending moment. Figure 12.3 illustrates a sheet bent to a cylinder of radius R. The film and the substrate have thicknesses d_f and d_s and Young's moduli Y_f and Y_s. When the sheet is bent, the top surface is in tension, and the bottom surface is in compression. One surface inside the sheet, known as the neutral surface, has no strain. The strain in the top surface ε_{top} equals the distance from the neutral surface divided by R. Typical silicon TFT materials and steel or glass have about the same Young's modulus. Consequently, the neutral surface is the mid-surface of the sheet, and the strain in the top surface is given by

$$\varepsilon_{\text{top}} = \left(d_f + d_s\right)/2R. \tag{12.8}$$

The minimum allowable radius of curvature scales linearly with the total thickness, assuming that the transistors fail upon reaching a critical value of strain.

Now let us look at the TFT film on a compliant substrate such as plastic. The film and the substrate have different elastic moduli ($Y_f > Y_s$), so that the neutral surface shifts from the mid-surface and toward the film. Consequently, the strain on the top surface is reduced, as given by

$$\varepsilon_{\text{top}} = \left(\frac{d_f + d_s}{2R}\right)\frac{\left(1 + 2\eta + \chi\eta^2\right)}{(1+\eta)(1+\chi\eta)}, \tag{12.9}$$

where $\eta = d_f / d_s$ and $\chi = Y_f / Y_s$. Figure 12.5 plots the normalized strain in the film *vs.* d_f / d_s. Two kinds of substrates are compared: steel ($Y_f / Y_s \cong 1$) and plastic ($Y_f / Y_s \cong 100$). For given R and d_f / d_s, the compliant substrate can reduce the strain by as much as a factor of five.

The strain in a circuit is further reduced if it is placed in the neutral surface itself, sandwiched between the substrate and an encapsulation layer of suitable Young's modulus and thickness, Y_e and d_e. When the stiffness of the circuit proper is negligible, the circuit comes to lie in the neutral surface if

$$Y_s d_s^2 = Y_e d_e^2. \tag{12.10}$$

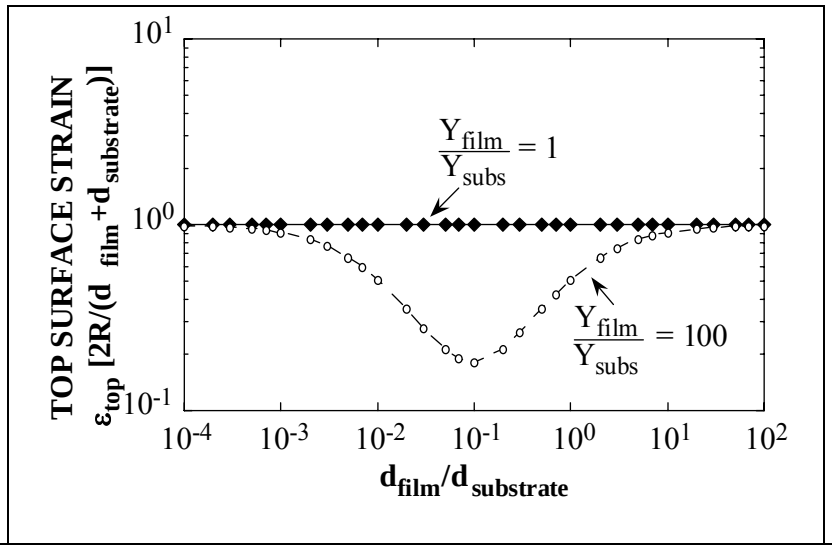

Figure 12.5 Normalized strain in the film as a function of film/substrate thickness ratio. Two types of substrates are illustrated: glass or steel ($Y_f / Y_s \cong 1$) and organic polymer ($Y_f / Y_s \cong 100$). (Suo et al., 1999)

In this case bending does not add any strain to the circuit. Consequently, the bending curvature is no longer limited by the failure strains of the transistor materials, but by those of the substrate and the encapsulation. When low modulus, small thickness substrate and encapsulation are used, the whole structure can be bent to extremely small radii. Because a-Si TFTs can be made on substrates as thin as 3 μm (Ma and Wagner, 1999), foldable TFT backplanes are possible.

To compare the data for a given strain ε between bending and stretching experiments, we calculate the strain ε under stretching from the load F measured with a load cell, using the following equation:

$$\varepsilon = \frac{F}{Y_f A_f + Y_s A_s} \tag{12.11}$$

where A_f and A_s are the cross-sectional areas of film and substrate. Equation (12.11) assumes a linear relationship between stress and strain (elastic deformation), which in our experience is a reasonable assumption for a-Si TFTs on a polyimide substrate.

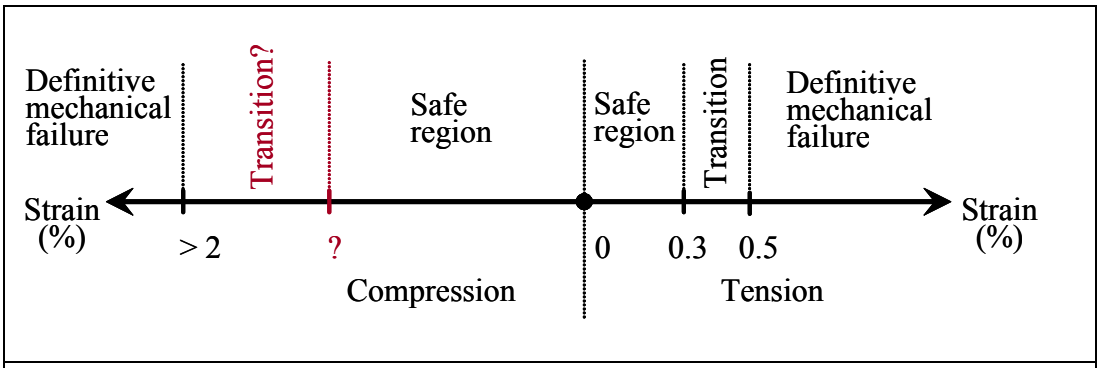

Figure 12.6 Summary of the response of a-Si TFTs to mechanical strain

12.4 Effects of mechanical strain on a-Si TFTs

a-Si TFTs respond to increasing mechanical strain by elastic deformation followed by fracture (E.Y. Ma, 1997, H. Gleskova, 1999, Gleskova, 2003, Gleskova et al., 1999). In measurements of TFTs on organic polymer substrates transition regimes are found, where the TFT fails but electrical function is restored when the strain is reduced (H. Gleskova, 2002). This phenomenon, which can cause confusion in tests, is believed to result from the electrical opening and closing of a crack in the TFT channel. The safe regimes of elastic deformation and the regimes of temporary and definitive failure explored by experiments are laid out in Figure 12.6.

Under elastic deformation up to fracture the transport properties of the TFT change reversibly (Gleskova et al., 1999, Gleskova, 2003). The electron mobility is reduced by compressive strain and is raised by tensile strain as shown in Figure 12.7. These mobility changes correlate with a broadening or steepening of the conduction band tail in a-Si (Gleskova et al., 2002).

a-Si TFTs can be strained more in compression than in tension. The theory of fracture of stiff films on stiff substrates provides a guide to explaining this difference in critical (fracture) strains (Suo, 2001). In tension the TFTs fail by crack propagation from pre-existing defects. In compression they fail by delamination followed by buckling and fracture. Fracture under tensile stress is illustrated in Figure 12.8(a), where a crack propagates from a pre-existing flaw. Equation (12.12) gives the condition for crack formation. The dimensionless constant χ depends on the elastic constants of the film and the substrate, and can be very large for a stiff film on a compliant substrate. Γ is the specific surface energy in the crack. However, Equation (12.12)

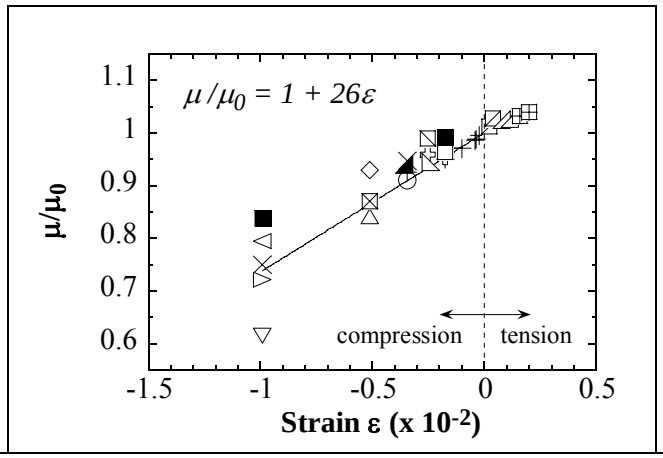

Figure 12.7 Electron mobility in a-Si TFTs plotted as a function of strain. Each symbol represents a different TFT. Empty and full symbols correspond to TFTs with the bending direction parallel and perpendicular to the source-drain current path, respectively. The linear fit is for TFTs with the bending direction parallel to the source-drain current path. (Gleskova et al., 2002)

provides only a qualitative guide, because experiments with glassy materials show that cracks can propagate at a critical stress much higher than that predicted by Equation (12.12). It agrees qualitatively with the observation that films crack more easily as their thickness is built up.

$$2\chi\frac{(1-\upsilon_f)\sigma_f^2 d_f^2 l}{Y_f} > 2\Gamma d_f \qquad (12.12)$$

Fracture under compressive stress, which is illustrated in Figure 12.8(b), occurs if the film debonds from the substrate. If the debonded area is sufficiently large, the film buckles and then fractures. The critical debonding length for buckling is given by Equation (12.13).

$$l_c = \frac{\pi d_f}{\sqrt{3(1-\upsilon_f^2)}}\sqrt{\frac{Y_f}{\sigma_f}} \qquad (12.13)$$

Estimates of critical debonding length for a-Si TFTs on Kapton polyimide show that for $Y_f/\sigma_f = 0.02$, $l_c \approx 10 \cdot d_f$. For a d_f = 1-μm thick device film, the critical debonding length $l_c \approx 10$ μm. In structures fabricated in a clean room this would be an unusually large defect. Therefore TFT/substrate structures are robust under compression. TFTs under compression have been observed to fracture if the substrate underneath first ruptures under the corresponding tensile strain that it experiences. (Suo, 2001, Kattamis, 2004)

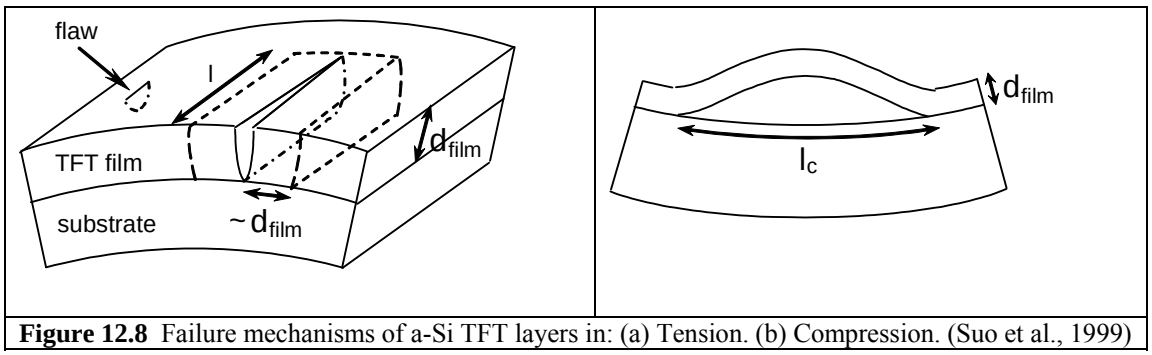

Figure 12.8 Failure mechanisms of a-Si TFT layers in: (a) Tension. (b) Compression. (Suo et al., 1999)

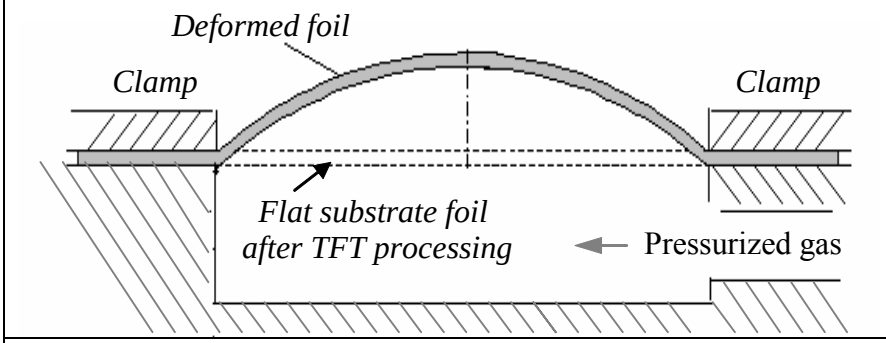

Figure 12.9 Apparatus for shaping a flat TFT backplane to a dome (Hsu et al., 2002b)

Cracking of device layers on polymer substrates can be suppressed by cutting the films into islands to expose the bare substrate. When TFT backplanes are to be shaped to conformal surfaces the TFTs must be placed on rigid device islands.

12.5 Shaping of TFT backplanes by plastic deformation

The deformation of a TFT backplane from a flat to a conformal surface may require a large, tensile, plastic deformation. A flat disk can be shaped to a dome by applying gas pressure to one side of the disk as shown in Figure 12.9 (Hsu et al., 2000, Hsu et al., 2002b, Hsu et al., 2004). Because the strain easily may exceed the critical fracture strain of a-Si TFTs of 0.3% to 0.5% shown in Figure 12.6, the TFTs are placed on rigid island platforms (Hsu et al., 2002a). Rows of such islands can be seen in Figure 12.1(b). The size and thickness of islands that can withstand deformation to a given radius (or field of view) of the dome are determined by experiment. The island size is of the order of the substrate thickness.

The contour plot of Figure 12.10 shows the radial strain distribution in an organic polymer substrate around one rigid island. For the calculation by finite element modeling, a 0.5-µm thick silicon island with 100-µm-diameter was placed in the center of a 200-µm diameter disk of a 50-µm thick Kapton E polyimide substrate (Hsu, 2003) . The substrate was stretched radially at its periphery to an average biaxial tension of 6%. Because the island is only 0.5-µm thick, its cross section is too thin to be seen in Figure 12.10. The strain in the island is the same as in the island/substrate interface. The strain in the substrate underneath the island is pinned to low values by the high elastic modulus of the island. Deep below the island the strain increases, and it is large in the exposed substrate surface.

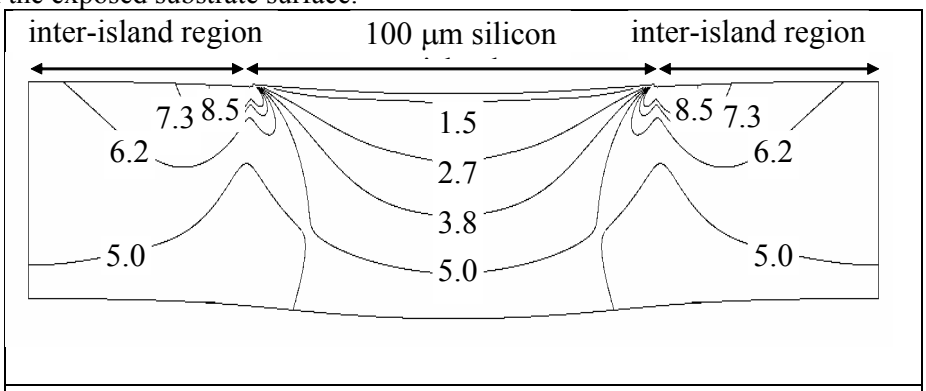

Figure 12.10 Contour plot of the radial strain (in %) a polyimide substrate with a round silicon island, after stretching. See text for details. (Hsu, 2003)

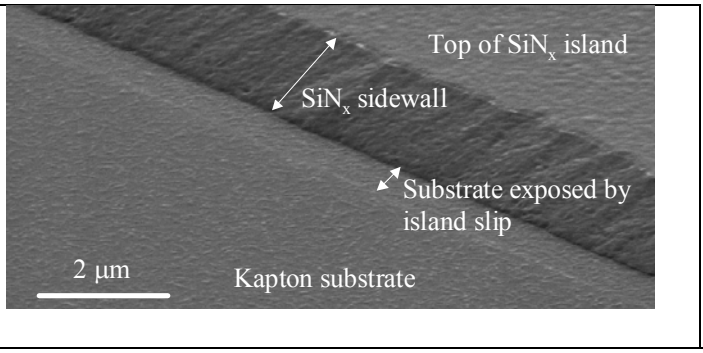

Figure 12.11 SEM micrograph of the edge of a SiN_x island on a polyimide foil after deformation of the foil to a dome. The substrate exposed by island slip is seen at the edge of the island. (Bhattacharya, 2003)

As long as the strain in the island is kept below its critical fracture strain, the island and the devices placed on it remain intact. However, islands and devices do exhibit secondary effects, of which we discuss two: slip of the island edge, and compressive buckling of the island.

The strain concentration in the polymer substrate at the edge of the island, evident in Figure 12.10, can cause the island edge slip on the substrate. Substrate newly exposed by this slip is visible in the scanning electron micrograph of Figure 12.11, which shows the edge of a SiN_x island on a Kapton E polyimide substrate. (Bhattacharya, 2003) The slip may be accompanied
by local delamination of the island at its perimeter. Both slip and delamination present challenges to the fabrication of electrically continuous interconnect.

When the force (pressure) that expands the substrate disk to the dome is released, the dome partly relaxes by elastic snap-back. This relaxation corresponds to the step from point 2 to point 3 shown in Figure 12.12. It puts the rigid islands in compression. The ensuing buckling of the islands has been observed by optical microscopy (Bhattacharya, 2003) and atomic force microscopy (Salomon, 2003), and the compressive strain is manifest in a reduced electron mobility of the a-Si TFTs that are fabricated on the islands (Hsu et al., 2004).

As illustrated by Figure 12.8(a) TFTs fail in tension by brittle fracture, which can be suppressed by passivation of the flaws on which cracks nucleate. Some evidence suggests that

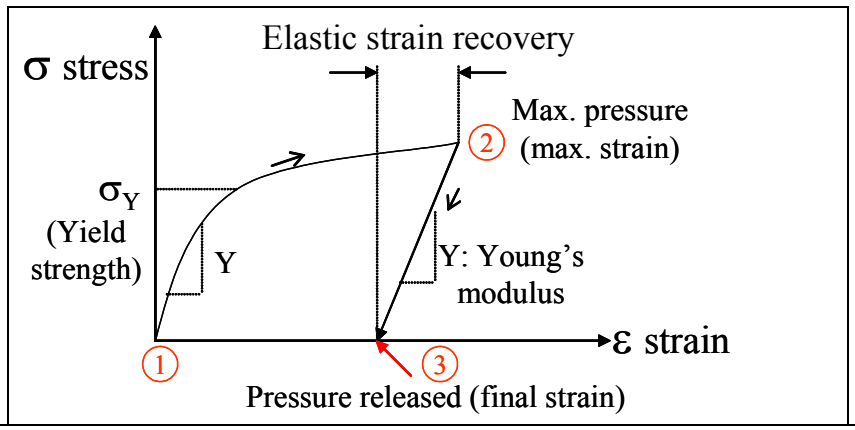

Figure 12.12 Stress-strain diagram illustrating the tensile shaping of a polymer substrate (step 1 to 2) followed by elastic snap-back (step 2 to 3) (Hsu et al., 2002)

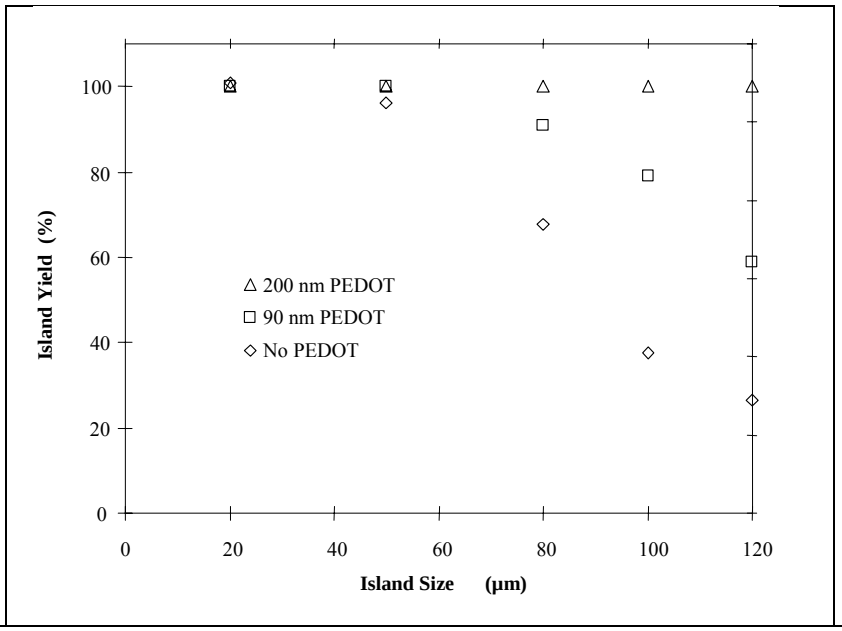

Figure 12.13 Yield of crack-free ITO islands on PET vs. island size, without PEDOT cover and for two different thicknesses of PEDOT coverage (Bhattacharya et al., 2004)

TFTs can be passivated by organic overlayers. Quantitative evidence for such passivation comes from recent work with islands of indium tin oxide (ITO), also a brittle material. Figure 12.13 shows the yield of intact square islands of 150-nm thick ITO on a 175-μm thick substrate of polyethylene terephthalate (PET). The islands are equispaced and cover 44% of the substrate. A 6-cm diameter disk covered with islands was deformed to a dome with 10 cm radius of curvature, which produced an average strain of 1.6%. The yield of crack-free ITO islands is seen to decrease with increasing island size. The yield is raised noticeably when the entire surface is coated with a blanket organic overlayer, and more so when this overlayer is made thick. While in this particular case the overlayer is of poly-3,4-ethylenedioxythiophene (PEDOT), the effect has been observed with other organic overlayers as well (Bhattacharya et al., 2004)

12.6 Stiff TFT films on organic polymer substrates: case studies

We use three examples to illustrate the mechanics of stiff device films on compliant substrates: (1) Evaluation of built-in stress in a device film; (2) Control of mask overlay alignment by adjustment of this built-in stress; and (3) Determination of electrical failure of TFTs after bending to progressively smaller radii of curvature.

12.6.1 Evaluation of built-in stress in a device film

Film stress is extracted from the radius of curvature R using Equation (12.7), instead of Equation (12.4) for stiff samples. On sufficiently rigid samples R can be measured with a surface profiler. In samples with low mechanical strength the laser reflection technique can be used. Samples with low strength may bend under their own weight. Then R can be measured when the samples are stood on end as shown in Figure 12.14. (Cheng, 2004) If R is not uniform an average must be estimated.

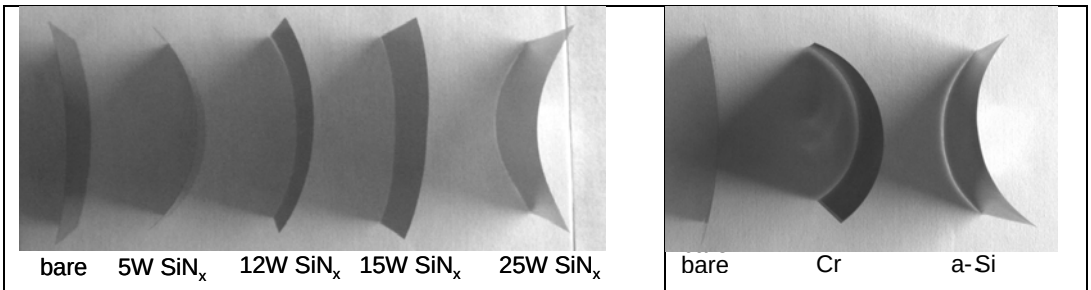

Figure 12.14 Stress-induced curvatures of (a) SiN_x films deposited at various deposition powers and of (b) Cr and a-Si films, all on 51-μm thick Kapton E polyimide substrates. The 300-nm (5W) to 500-nm (25W) thick SiN_x and the 250-nm a-Si films were deposited at 150°C; the thermally evaporated Cr film is 80 nm thick. The built-in stress in the SiN_x film can be adjusted by deposition power. The built-in stresses of Cr and a-Si:H films are tensile and compressive, respectively. The films are on the left side of the substrates (Cheng, 2004)

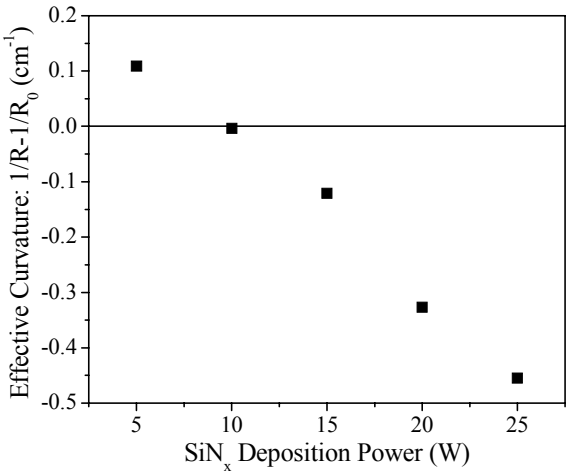

Figure 12.15 Effective radius of curvature produced by PE-CVD deposition of 300-nm thick SiN_x at 150°C on 51-μm thick Kapton E polyimide substrates. Substrates pre-heated for 50 minutes in vacuum, and radii measured after 30-minute cooling in vacuum, at room temperature and RH = 29% (Cheng, 2004)

The net curvature produced in the samples $K = 1/R$, as in the samples of Fig. 12.14, is the sum of the "effective" curvature introduced by processing and the curvature $K_0 = 1/R_0$ of the as-received, bare, substrate. (A sheet of polymer foil cut from a roll usually is curved.) Values for the effective curvature $1/R - 1/R_0$ for samples with PE-CVD SiN_x films on Kapton E polyimide are plotted in Figure 12.15.

The sign of the radius of curvature R is defined as negative when films faces outward (convex) because the film is in compression, i.e., $\varepsilon_f < 0$. R is positive when the film faces inward (concave) because the film is in tension, i.e., $\varepsilon_f > 0$. This sign definition is opposite to that in bending by an externally applied moment, because we now are dealing with an internally produced, film-stress induced, curvature. The total mismatch strain, ε_M is given by

$$\varepsilon_M = \varepsilon_{th} + \varepsilon_{ch} + \varepsilon_0 \qquad (12.14)$$

where the thermal mismatch strain, ε_{th}, is given by

$$\varepsilon_{th} = \left(\alpha_f - \alpha_s\right) \times \left(T_{dep} - T_{room}\right), \tag{12.15}$$

and the mismatch strain produced by moisture absorption, ε_{ch}, in a sample that was dried completely before vacuum processing and afterwards was brought into air for measuring *R*, is given by

$$\varepsilon_{ch} = -\left(\beta_f - \beta_s\right) \times \%RH\,. \tag{12.16}$$

We use the symbol β for the coefficient of humidity expansion, and %RH stands for percent of relative humidity. Now we are able to approximate the total mismatch strain ε_M from the measured radius of curvature *R*, using the tabulated material properties *Y* and ν, and the thicknesses *d*:

$$\varepsilon_M = \frac{\left(\overline{Y}_s d_s^2 - \overline{Y}_f d_f^2\right)^2 + 4\overline{Y}_f \overline{Y}_s d_f d_s \left(d_f + d_s\right)^2}{6\left(1+\nu\right)\overline{Y}_f \overline{Y}_s d_f d_s \left(d_f + d_s\right)} \left(\frac{1}{R} - \frac{1}{R_0}\right). \tag{12.17}$$

where ν is the average value of ν_f and ν_s. (12.17) is identical to (12.7), except that we take into account the radius of the substrate prior to film deposition, R_0. Then we subtract from ε_M the thermal mismatch strain ε_{th} and the humidity expansion strain ε_{ch} in (12.14). Left over is the built-in strain ε_0 produced by film growth as shown in Figure 12.16.

Table 12.2 Data used in the extraction of the built-in stress in SiN_x films on Kapton E foil substrates

	Kapton E	SiN_x deposited at 150°C ($T_{dep} - T_{room}$ = 125°C)
Young's modulus	Y_s = 5.3 GPa	Y_f = 210 GPa
Poisson's ratio	ν_s = 0.32	ν_f = 0.25
Biaxial stress modulus $Y^* = \frac{Y}{1-\nu}$	Y_s^* = 7.8 GPa	Y_f^* = 280 GPa
Plane strain modulus $\overline{Y} = \frac{Y}{1-\nu^2}$	$\overline{Y}_s$ = 5.9 GPa	$\overline{Y}_f$ = 224 GPa
Coefficient of thermal expansion	α_s = 16 ppm/K	α_f = 2.7 ppm/K
Coefficient of humidity expansion	β_s = 8 ppm/%RH	β_f = 0 ppm/%RH
Radius of curvature of substrate as received	R_0 = 14.3 cm	

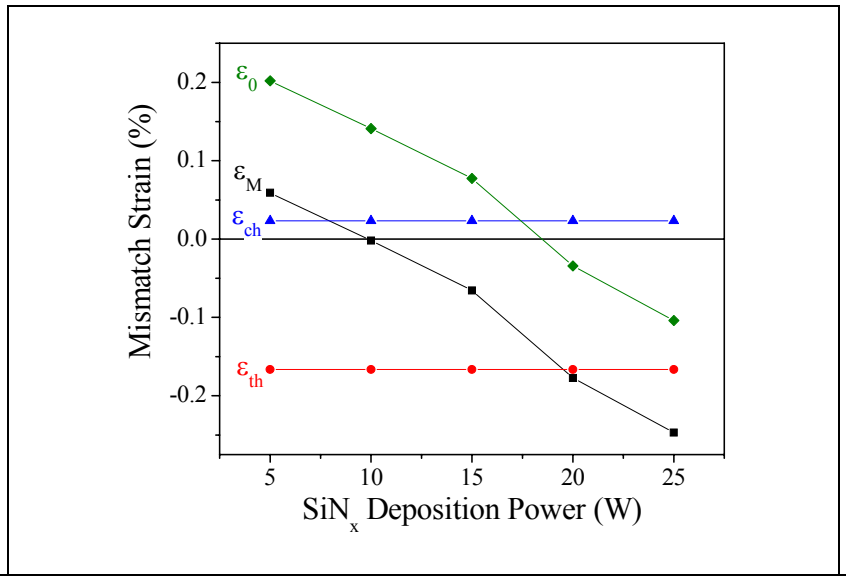

Figure 12.16 Mismatch strain components calculated or extracted for the samples of Figure 12.15. The horizontal line denotes zero strain. The film is under tension at positive strain and compression at negative strain. (Cheng, 2004a)

Next we calculate the built-in stress in the film after the deposition is completed while the sample is still held flat in a frame. Assuming that the built-in strain, ε_0, does not change during cooling and/or after releasing from the frame, the built-in stress in the film, σ_0^f, can be expressed by (12.18) and an example is shown in Figure 12.17.

$$\sigma_0^f = \frac{Y_f^* Y_s^* d_s}{Y_f^* d_f + Y_s^* d_s} \times \varepsilon_0 \qquad (12.18)$$

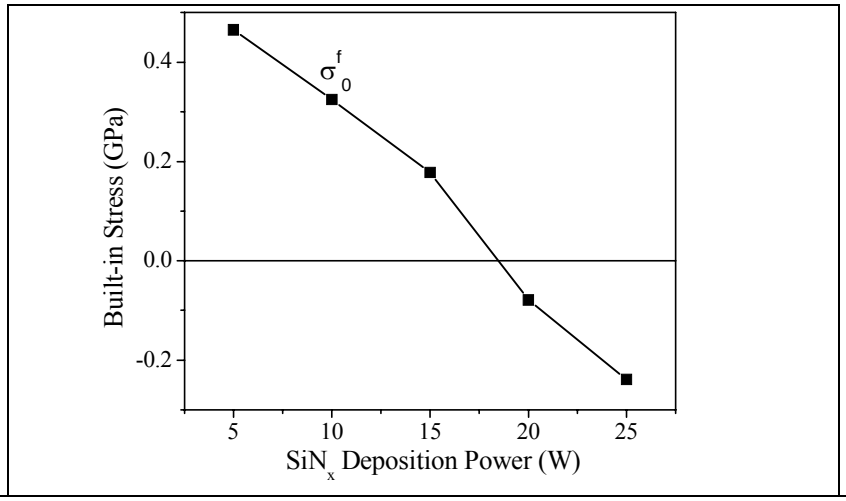

Figure 12.17 Built-in stress in the film when the sample is held in a frame. The stress is calculated or extracted for the samples of Figure 12.15. The horizontal line denotes zero stress. Positive stress stretches and negative stress compresses the film.

12.6.2 Control of mask overlay alignment by adjustment of built-in stress

Varying curvature corresponds to varying size of the flattened sample. Stress-induced curvature that varies during backplane fabrication causes misalignment in overlay registration. It is possible to improve the overlay registration by stress management in the device layers. (Cheng, 2004)

TFTs were fabricated in the non-self-aligned, back-channel-etched geometry of Figure 12.2(b) on 2-mil (51-µm) thick, 70-mm x 70-mm square Kapton E polyimide substrates. The samples were carried as free-standing films through most of the process steps, except in photolithography when they were temporarily bonded to glass by the surface tension of water. (Figure 12.16 shows that the uptake and release of water by the polyimide has a secondary effect compared to built-in and thermal stress.) We monitored the degree of misalignment between the first and second photolithography levels, i.e., the bottom gate and the source/drain. Their alignment is crucial to setting source/gate and gate/drain overlaps. At both levels we aligned to a mark at the center of the substrate, and measured the misalignment of four marks lying at the corners of a 52-mm x 52-mm square, with each mark close to a corner of the substrate.

Between the two photolithographic steps fell the deposition at 150°C of the silicon stack, composed of (i) 300-nm SiN_x gate dielectric, (ii) 200-nm i a-Si channel, (iii) 50-nm n^+ a-Si source/drain and (iv) Cr source/drain contact. To quantify the stress compensation we kept all these layers the same, except for intentionally varying the built-in stress in the gate SiN_x from tensile to compressive. This we did by tuning the deposition power from low to high, 5W, 12W, 25W (22, 53, 89 mW/cm^2), which results in an effective stress in the film stack ranging from highly tensile to slightly tensile to slightly compressive (see Figure 12.14). The corresponding overlay misalignment is illustrated by Figure 12.18. The sample is seen to shrink much with a 5W gate SiN_x, shrink slightly at 12W, and expand slightly at 25W. The TFT transfer characteristics of Figure 12.19 show that varying the deposition power has only a slight effect on electrical performance: I_{on} at V_G = 25V drops slightly as the tensile stress is reduced, in agreement with the mobility change shown in Figure 12.7. Thus adjusting stress in the SiN_x layer is a realistic technique for controlling overlay alignment for a-Si TFT circuits on a compliant substrate.

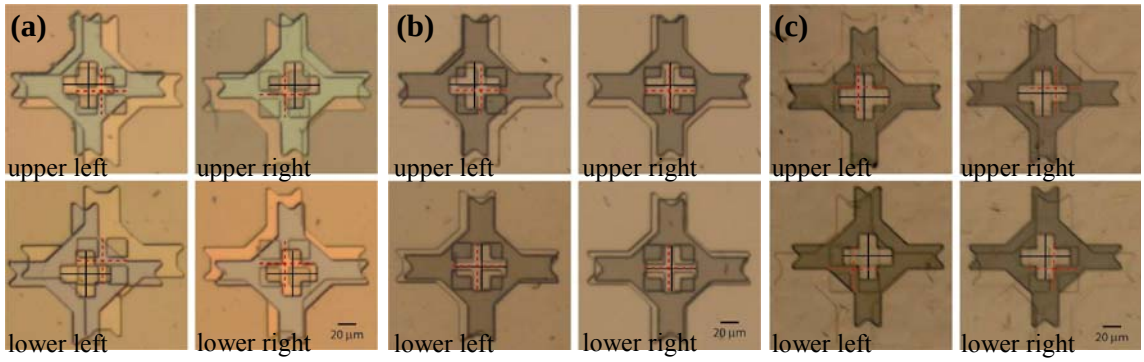

Figure 12.18. Overlay misalignment between the first, bottom-gate, and second, source/drain, photolithography levels in back-channel etched a-Si TFT process with (a) 5W gate SiN_x, (b) 12W gate SiN_x, and (c) 25W gate SiN_x. The frames lie 52 mm apart near the corners of the 70-mm square substrate. The dashed crosses mark the center at the gate mask level and the solid crosses the centers at the source/drain mask levels. The sample is seen to shrink substantially with 5W SiN_x, slightly with 12W SiN_x, and expand substantially with 25W SiN_x. (Cheng, 2004)

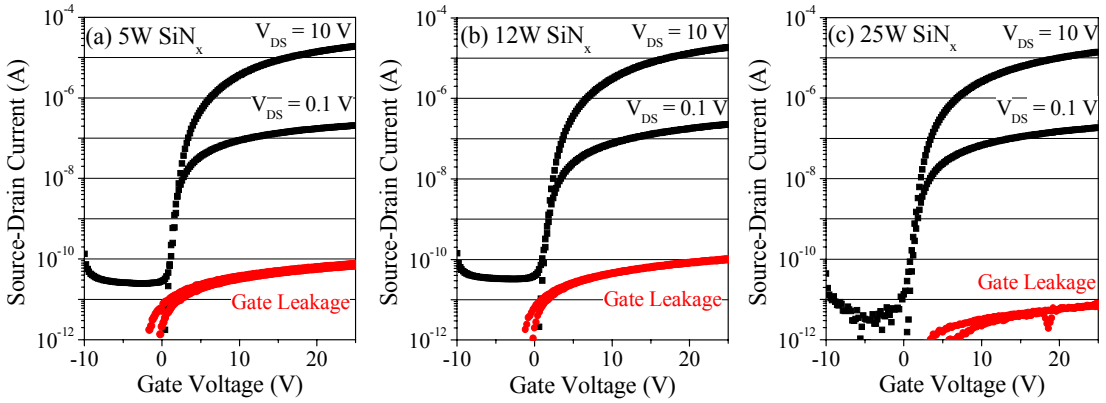

Figure 12.19. Transfer characteristics of TFTs of Figure 12.18(a), (b), and (c). The TFT gates are 80 μm wide and 10 μm long (Cheng, 2004)

12.6.3 Determination of electrical failure of a-Si TFTs after bending

Because elastic deformation has a small and reversible effect on the electrical performance of a-Si TFTs, the critical radius where the TFTs fracture may be all the information that is needed. The only mechanical test needed may be bending the backplane to progressively sharper radii, and in between measure the TFT characteristics on the flattened substrate. (Gleskova et al., 1999) We bent TFTs on Kapton substrates outward, top surface of Figure 12.3, or inward, bottom surface of Figure 12.3. Single TFTs were bent to decreasing R, beginning with R = 4 mm down to R = 0.5 mm. The TFT was stressed for one minute at each bending radius, and then was released, flattened and re-measured. Figure 12.20 summarizes the effects of inward/compressive (a) and outward/tensile (b) bending on TFT performance. The top graphs in each subset show the on-current I_{on}, the off-current I_{off}, and the gate-leakage current I_{leak} as functions of the radius of curvature. Likewise, the bottom graphs in each subset show the threshold voltage V_T and the saturated electron mobility μ_n, calculated from the transfer characteristic at source-drain voltage V_{ds} = 10 V. Differences between the "Initial" characteristics reflect spread between as-fabricated TFTs.

Inward/compressive bending down to R = 0.5 mm, left column of Figure 12.20, shows that the TFT can be compressed by at least 2% without failing. In outward/tensile bending, right column of Figure 12.20, no substantial changes are observed down to R = 1 mm (0.5% strain). After bending to sharper radii some TFTs had failed. The electrical failure was caused by periodic cracks in the TFT island that run perpendicular to the bending direction.

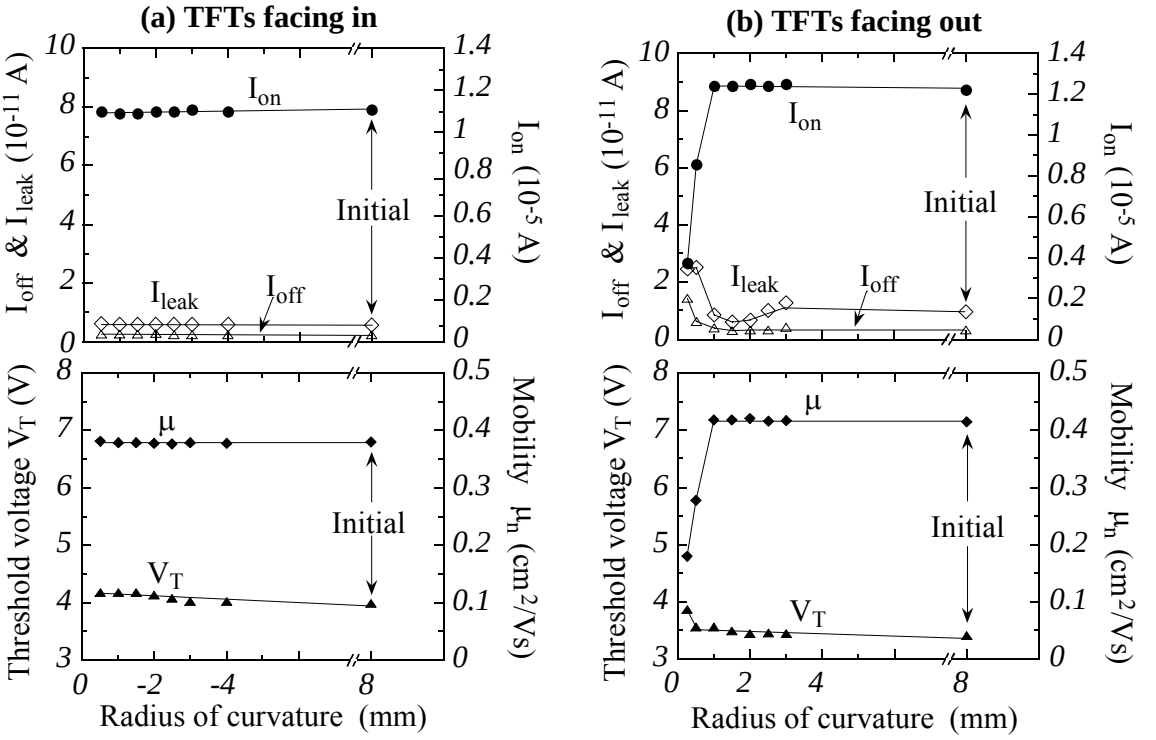

Figure 12.20 On-, source-gate leakage, off-currents, electron mobility, and threshold voltage in the saturation regime as functions of bending radius. I_{off} is the smallest source-drain current at V_{ds} = 10V, I_{on} is the source-drain current for V_{ds} = 10 V and the gate voltage V_{gs} = 20 V, and I_{leak} is the source-gate current for V_{ds} = 10 V and V_{gs} = 20 V. Outward bending R is defined positive, inward bending negative. The as-fabricated radius, before bending was 8 mm. Differences between the "Initial" characteristics reflect spread between as-fabricated TFTs. (Gleskova et al., 1999)

12.7 Summary and outlook

Research on flexible TFT backplanes remains focused on materials and processes for backplane fabrication. Initial exploration of the limits of bending and shaping made clear that TFT backplanes can be bent tightly and even folded. Work on backplane mechanics now has moved to design of materials and processes for film integrity, and control of substrate dimensions, during fabrication. Accurate control of substrate dimensions by mounting on temporary carriers for production on plates and eventually roll-to-roll is an important goal. Detailed experiments and theory on the mechanics of layered and patterned structures will help design locally stable films and dimensions. Further layering and lamination of the TFT backplane to a finished product will raise mechanical issues that are similar to those encountered in backplane mechanics. Conformally shaped and elastomeric TFT backplanes will continue to provide demanding subjects for experimental and theoretical mechanics, the latter challenged by the need for providing simple if approximate analytical tools. The gradual introduction of organic electronics will expand the mechanical boundaries of TFT backplanes and undoubtedly will present new tasks to the researcher.

Many signals indicate that the mechanics of electronic surfaces will remain important and demanding for a long time to come: the rapid growth of the flat panel display industry; the growing number of techniques for fabricating thin-film electronics by potentially inexpensive processes; the demonstration of new display, sensor, and actuator frontplane functions; and

widespread interest in large screens, unbreakable and wearable electronics, e-textiles, and electronic skins.

Literature references **[Note: references not cleaned up – for corrections see proofs]**

Bhattacharya, R. (2003)**,** Princeton University, unpublished work.

Bhattacharya, R., Wagner, S., Tung, Y.-J., Esler, J. and Hack, M. (2004) In *Conf. Record 2004 IEEE International Electron Devices Meeting*San Francisco, 13-15 Dec. 2004, pp. 15.6.1-15.6.4.

Bonse, M., Huang, J. R., Wronski, C. R. and Jackson, T. N. (1998) In *Conf. Record 1998 International Electron Devices Meeting*IEEE, pp. 253-256.

Brody, T. P. (1996) *Journal of the SID,* **4,** 113-127.

Burns, S. G., Shanks, H., Constant, A., Gruber, C., Schmidt, D., Landin, A. and Olympie, F. (1997) In *The Electrochemical Society Proceedings*, Vol. 96-23 (Ed, Kuo, Y.), pp. 382-390.

Chen, Y. (2001) *E Ink Corp., personal communication*.

Cheng, I.-C. (2004) Princeton University, unpublished work.

Constant, A., Burns, S. G., Shanks, H., Gruber, C., Landin, A., Schmidt, D., Thielen, C., Olympie, F., Schumacher, T. and Cobbs, J. (1994) In *The Electrochemical Society Proceedings*, Vol. 94-35 (Ed, Kuo, Y.), pp. 392-400.

Gleskova, H. (2003) Princeton University, unpublished work.

Gleskova, H., Ma, E. Y., Wagner, S. and Shen, D. S. (1996) In *Dig. Tech. Papers, 1996 Display Mfg. Technical Conference*SID, Santa Ana, CA, San Jose, CA., pp. 97-98.

Gleskova, H., Wagner, S. and Shen, D. S. (1995) *IEEE Elec. Dev. Lett.,* **16,** 418-420.

Gleskova, H., Wagner, S., Soboyejo, W. and Suo, Z. (2002) *J. Appl. Phys.,* **92,** 6224-6229.

Gleskova, H., Wagner, S. and Suo, Z. (1998) *Mat. Res. Soc. Symp. Proc.,* **508,** 73-78.

Gleskova, H., Wagner, S. and Suo, Z. (1999) *Appl. Phys. Lett.,* **75,** 3011-3013.

Gray, D. S., Tien, J. and Chen, C. S. (2004) *Advanced Materials,* **16,** 393-397.

Hsu, P.-H. I. (2003) Ph.D. thesis, Princeton University.

Hsu, P.-H. I., Huang, M., Gleskova, H., Xi, Z., Z. Suo, Wagner, S. and Sturm, J. C. (2004) *IEEE Transactions on Electron Devices,* **51,** 371-377.

Hsu, P.-H. I., Huang, M., Wagner, S., Suo, Z. and Sturm, J. C. (2000) *Mat. Res. Soc. Symp. Proc.,* **621,** Q8.6.1-Q8.6.6.

Hsu, P. I., Bhattacharya, R., Gleskova, H., Huang, M., Xi, Z., Suo, Z., Wagner, S. and Sturm, J. C. (2002) *Applied Physics Letters,* **81,** 1723-1725.

Hsu, P. I., Gleskova, H., Bhattacharya, R., Xi, Z., Suo, Z., Wagner, S. and Sturm, J. C. (2002c) In *Mat. Res. Soc. Spring 2002 Meeting*, Vol. Paper G1.8 San Francisco, CA.

Jones, B. L. (1985) In *J. Non-Cryst. Solids*, Vol. 77-78, pp. 1405-1408.

Kattamis, A. (2004)**,** Princeton University, unpublished work.

Lacour, S. P., Wagner, S., Huang, Z. and Suo, Z. (2003) *Appl. Phys. Lett.,* **82,** 2404-2406.

Lueder, E., Muecke, M. and Polach, s. (1998) In *18th International Display Research Conference Asia Display '98*SID, pp. 173-177.

Lumelsky, V., Shur, M. and Wagner, S. (2001) *IEEE Sensors Journal,* **1,** 41-51.

Ma, E. Y., Theiss, S. D., Lu, M. H., Wu, C. C., Sturm, J. C. and Wagner, S. (1997) In *Conf. Record 1997 IEEE International Electron devices Meeting*, pp. 535-538.

Ma, E. Y. and Wagner, S. (1999) *Appl. Phys. Lett.,* **74,** 2661-2662.

Pai-hui I. Hsu, M. H., Sigurd Wagner, Zhigang Suo, and J. C. Sturm (2000) *Mat. Res. Soc. Symp. Proc.,* **621**.

Parsons, G. N., Yang, C. S., Arthur, C. B., Klein, T. M. and Smith, L. (1998) In *Flat Panel Display Materials*, Vol. 508 (Eds, Parsons, G. N., Tsai, C. C., Fahlen, T. S. and Seager, C. H.) Materials Research Society Symposium Proceedings, pp. 19-24.

Salomon, A. (2003) Princeton University, M.Eng. thesis.

Sandoe, J. N. (1998) In *SID 1998vInternational Symposium Digest of Technical Papers*, Vol. 29 SID, Santa Ana, CA, pp. 293-296.

Spear, W. E. and Heintze, M. (1986) *Phil. Mag. B,* **54,** 343-358.

Suo, Z. (2001) In *Encyclopedia of materials : science and technology* Elsevier, 2nd. ed., Amsterdam, London, pp. 3290-3296.

Suo, Z., Ma, E. Y., Gleskova, H. and Wagner, S. (1999) *Appl. Phys. Letters,* **74,** 1177-1179.

Theiss, S. D., Carey, P. G., Smith, P. M., Wickboldt, P., Sigmon, T. W., Tung, Y. J. and King, T.-J. (1998) In *IEEE 1998 Int. Electron Devices Meeting Tech. Digest*, pp. 257-260.

Theiss, S. D. and Wagner, S. (1996) *IEEE Electron Device Letters,* **17,** 578-580.

Timoshenko, S. P. and Goodier, J. N. (1970) *Theory of Elasticity,* McGraw-Hill, New York.

Wagner, S., Gleskova, H., Sturm, J. C. and Suo, Z. (2000) In *Technology and Applications of Hydrogenated Amorphous Silicon*(Ed, Street, R. A.) Springer, Berlin, pp. 222-251.

Wagner, S., Lacour, S. P., Jones, J., Hsu, P.-H. I., Sturm, J. C., Li, T. and Suo, Z. (2004) *Physica E,* **25,** 326–334.

Young, N. D., Trainor, M. J., Yoon, S.-Y., McCulloch, D. J., Wilks, R. W., Pearson, A., Godfrey, S., Green, P. W., Rosendaal, S. and Hallworth, E. (2003), Vol. 769 Mat. Res. Soc. Symp. Proc., pp. H2.1.1-H2.1.12.